Vibration analysis of the CubeSat SPORT boom's through a flexible multibody model

Lorenzzo Q. Mantovani[1], Willer G. dos Santos[1], Flávio L. Cardoso-Ribeiro[1]

[1]*Dept. of Aeronautics and Aerospace Engineering, Aeronautics Institute of Technology (ITA)*
Praça Marechal Eduardo Gomes, 50 - Vila das Acácias, 12228-900, São Paulo, Brazil
lorenzzo.mantovani@gmail.com, willer@ita.br, flaviocr@ita.br

Abstract. SPORT (Scintillation Prediction Observation Research Task) is a 6U CubeSat being developed in a partnership among NASA, Aeronautics Institute of Technology (ITA), National Institute for Space Research (INPE) and several U.S. universities, with its launch planned for 2021. SPORT's scientific mission is the study of the pre-bubble conditions in space weather, which induce the formation of plasma bubbles; hence it has several instruments, with five of them positioned in four booms around the satellite. The boom's opening occurs through spring mechanisms soon after its ejection from the International Space Station (ISS). These same springs keep the boom's final position perpendicular to the satellite body since there are no mechanisms to lock the booms in place. Thus, periodic calibration maneuvers performed by the SPORT may induce vibration in both rigid and flexible modes of these booms, which can lead to interferences in the control system. These interferences can reduce the pointing accuracy of the satellite or even make the control system unstable, which supports the need to analyze them. This paper presents the modeling of the SPORT as a rigid body and its mechanisms as flexible bodies using a multibody approach, which allows simulating the boom's behavior in the space environment.

Keywords: Flexible multibody, Non-latching mechanism, Boom, CubeSat

1 Introduction

CubeSats have been used to complete the most diverse missions worldwide due to its known capabilities and positive aspects such as low cost, fast development, and standardized platform. With the advancement of its technology, its mission's goals changed from educational and technology demonstrations to encompass advanced scientific research. One example of such a case is the Scintillation Prediction Observations Research Task (SPORT) CubeSat with the goal of studying plasma bubbles, more specifically the pre-bubble condition through its instruments and radio occultation sensors, described in details in Charles et al. [1] . The mission is a cooperation among NASA, U.S. partner institutions, the National Institute for Space Research (INPE) and the Aeronautics Institute of Technolgy (ITA), which is responsible for the satellite platform.

SPORT platform follows the CubeSat standard and has six units (6U) which carry several scientific instruments: a Langmuir Probe (SLP), a Swept Impedance Probe (SIP), two Electric Field Probes (E-Fields), an Ion Velocity Meter sensor (IVM), a Magnetometer and a GPS Occultation system (CTESCS). While the IVM and CTESCS are mounted directly into the SPORT's central structure (HUB), the SLP, SIP, both E-Fields and the Magnetometer are placed on four booms around the satellite. The deployment of these booms occurs through torsional springs, which places them perpendicularly to the HUB.

After deployment, there is no latching mechanism to lock the booms in place with the springs responsible for maintaining the final position. Hence, the booms are constrained on one side by the HUB/mechanism structure and the other by the springs. This condition may cause the boom to vibrate and, consequently, inducing the HUB to oscillate impacting the Attitude and Determination Control System (ADCS). This impact may be more pronounced during the SPORT maneuvers used to calibrate its instruments, in which the satellite will periodically rotate twice around each axis.

In order to model this behavior, a multibody model was used since it is a powerful tool capable of describing complex body interactions in the most diverse situations. As an example, Rong et al. [2] describes several ongoing research in the multibody dynamics topics, such as reduction techniques, numerical methods, contact/collision dynamics, and its possible applications. Some cases include space systems, which require their structures to be

modeled as flexible bodies such as the variable-length tethers in Luo et al. [3] connecting three satellites in orbit, the use of piezoelectric actuators to suppress vibrations in antennae connected by flexible links by Ma et al. [4] or in Shi and Wang [5] who describes the tracking of a robotic manipulator coupled to a satellite with flexible appendages. Complex transient problems such as the thermally induced flutter faced by satellite solar panels are developed in Liu and Pan [6] or the sloshing dynamics under microgravity effect in space systems by Kong and Tian [7].

Thus, this work aims to present a modeling approach to simulate the SPORT HUB and its flexible booms using flexible multibody dynamics, which will provide a feasible tool to investigate the impact of the booms vibration on the ADCS on future works. Hence, Section 2 addresses the flexible multibody model used, and both the structural and mechanism model employed; Section 3 presents some results obtained with the method while Section 4 is the conclusion.

2   Flexible multibody model

This section addresses the flexible multibody model employed, separated into three distinct subsections. Subsection 2.1 describes the process to obtain the generalized Newton-Euler equations, and the equations to constrain the bodies relative motion. Subsection 2.2 defines the structural model used to approximate the booms' flexible behavior; Subsection 2.3 presents the spring model, which describes both the mechanisms and the collision behavior.

2.1   Flexible multibody dynamics

The general approach to obtain the equations of motion are developed based on Shabana [8], which describes the equations in detail, and begin considering the position vector of a point P on the body i - the notation adopted indicates the body by its superscript -, r_p^i:

$$r_P^i = R^i + A^i \bar{u}^i. \tag{1}$$

In eq. (1), R^i is the distance vector in $\Re^3$ of the Body Reference Frame, BRF, in the Inertial Reference System, IRS, (adopted equal to the commonly used Earth-Centered Inertial reference frame), written in the later one. A is a rotation matrix in $\Re^{3\times3}$ from the BRF to the IRS and $\bar{u}$ is the position vector in $\Re^3$ of point P written in the BRF system - which is indicated by the bar above it. For flexible bodies, the $\bar{u}$ vector can be decomposed in a rigid body component $\bar{u}_0$ and a flexible body component $\bar{u}_f$:

$$\bar{u}^i = \bar{u}_0^i + \bar{u}_f^i. \tag{2}$$

Figure 1a shows the relations presented by eq. (1) and eq. (2), while Fig. 1b describes the BRF^i ($X^i Y^i Z^i O$) used for each body. Although the image shows the origin of the mechanisms BRF at an arbitrary point along them, it was used in order to facilitate the visualization. The origins are at the base of the booms which connect to the spring mechanism (close to the HUB). The bodies are: HUB (1), E-Filed + (2), E-Field - (3), SIP (4) and SLP (5).

The flexible body component, $\bar{u}_f$, can be written as a function of the flexible body elastic coordinates, q_f^i, which leads to:

$$\bar{u}_f^i = S^i q_f^i. \tag{3}$$

Vector q_f^i is in the $\Re^n$ space while S^i is in the $\Re^{3\times n}$ space. The variable n is the number of flexible modes adopted for each body i. The time derivative of eq. (1) leads to

$$\dot{r}_P^i = \dot{R}^i + \dot{A}^i \bar{u}^i + A^i S^i \dot{q}_f^i \tag{4}$$

(a) Position of point P in body i. Adapted from Shabana [8]

(b) BRF of each body of the multibody model
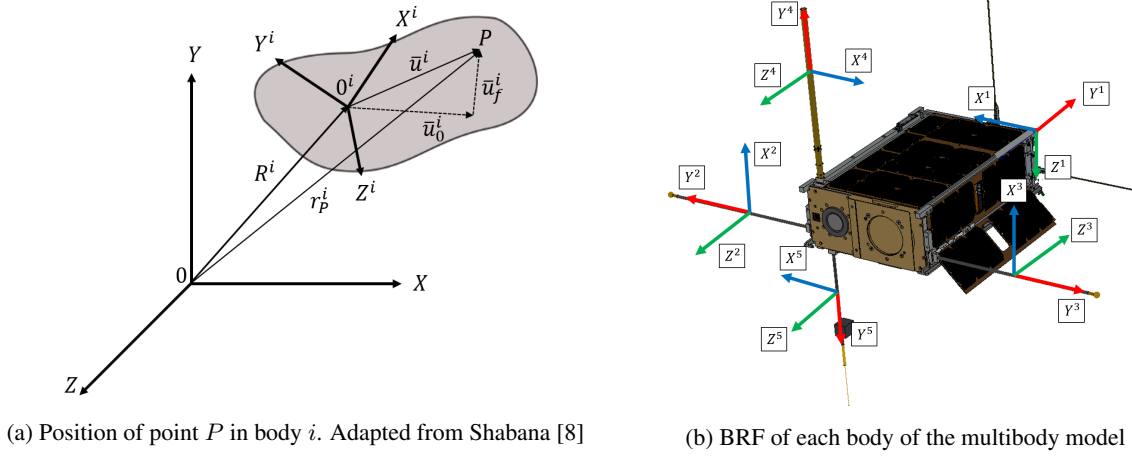
Figure 1. Reference systems used in model

since both $\bar{u}^i$ and S^i are constant. In order to facilitate further development, the following relation $\dot{A}^i \bar{u}^i = \tilde{u}^{i^T} \omega^i$ is used in which $\tilde{u}^i$ is the skew symmetric matrix of u^i in $\Re^{3\times3}$ space and ω^i is the angular velocity vector written in the IRF in $\Re^3$ space. Hence, eq. (4) can be rewritten to:

$$\dot{r}_P^i = \begin{bmatrix} \mathrm{I} & \tilde{u}^{i^T} & A^i S^i \end{bmatrix} \begin{bmatrix} \dot{R}^i \\ \omega^i \\ \dot{q}_f^i \end{bmatrix} = L^i \dot{q}^i. \tag{5}$$

Where L is a matrix in $\Re^{3\times3} \times \Re^{3\times n_\theta} \times \Re^{3\times n}$ and $\dot{q}^i$ is the vector of generalized velocities in $\Re^3 \times \Re^{n_\theta} \times \Re^n$ space. With the relation established in eq. (5), the generalized mass matrix for body i can be obtained from the kinetic energy T^i considering the body volume V^i and density ρ^i:

$$T^i = \frac{1}{2} \int_{V^i} \rho^i \dot{q}^{i^T} L^{i^T} L^i \dot{q}^i dV = \frac{1}{2} \dot{q}^{i^T} \int_V^i \rho^i L^{i^T} L^i dV \dot{q}^i = \frac{1}{2} \dot{q}^{i^T} M^i \dot{q}^i. \tag{6}$$

The mass matrix M is symmetric, and can be decomposed in smaller matrices:

$$M^i = \begin{bmatrix} m_{RR} & A^i \tilde{\bar{S}}_t^{i^T} & A^i \bar{S}^i \\ \left(A^i \tilde{\bar{S}}_t^{i^T} \right)^T & \bar{I}_{\theta\theta}^i & \bar{I}_{\theta f}^i \\ \left(A^i \bar{S}^i \right)^T & \left(\bar{I}_{\theta f}^i \right)^T & m_{ff}^i \end{bmatrix}. \tag{7}$$

The diagonal matrix m_{RR}^i in $\Re^{3\times3}$ represents the translational mass of the body, $\bar{I}_{\theta\theta}^i$ the inertia matrix in $\Re^{3\times3}$, and m_{ff}^i is the mass matrix associated with the modal shapes in $\Re^{n\times n}$. Matrices outside the main diagonal ($\tilde{\bar{S}}_t^{i^T}$, $\bar{S}^i$ and $\bar{I}_{\theta f}^i$) represents the coupling in translation, rotation and flexible body motion. The equations for the aforementioned matrices are shown by Schiavo et al. [9] for modal shapes, and Ferretti et al. [10] for both modal shapes and finite element methods.

It is necessary, with the already defined generalized mass matrix, to obtain the generalized forces acting on the system. Shabana [8] uses the Euler-Lagrange equation to obtain the forces associated with the Coriolis and gyroscopic component (Q_α^i) in $\Re^3$, and other two generalized force vectors, Q_R^i in $\Re^3$ space and Q_f^i in $\Re^n$ space:

$$\begin{aligned} Q_R^i &= -A^i [(\tilde{\bar{\omega}}^i \bar{S}_t^i) + 2\tilde{\bar{\omega}}^i S^i \dot{q}_f^i] \\ Q_\alpha^i &= -\bar{\omega}^i \times (\bar{I}_{\theta\theta}^i \bar{\omega}^i) - \dot{\bar{I}}_{\theta\theta}^i \bar{\omega}^i - \bar{\omega}^i \times (\bar{I}_{\theta f}^i \dot{q}_f^i) \\ Q_f^i &= -\bar{\omega}^i \times (\bar{I}_{\theta\theta}^i \bar{\omega}^i) - \dot{\bar{I}}_{\theta\theta}^i \bar{\omega}^i - \bar{\omega}^i \times (\bar{I}_{\theta f}^i \dot{q}_f^i). \end{aligned} \tag{8}$$

Then, the generalized forces acting on the system, Q^i, can be defined as:

$$Q^i = \begin{bmatrix} Q_R^i + Q_{R_{ext}}^i \\ Q_\alpha^i + Q_{\alpha_{ext}}^i \\ Q_f^i - K_{ff}^i q_f^i - D_{ff}^i \dot{q}_f^i \end{bmatrix}. \tag{9}$$

Where K_{ff}^i is the stiffness matrix of the flexible structure obtained from the virtual work of the elastic forces, and D_{ff}^i the structural damping matrix. Also, $Q_{R_{ext}}^i$ and $Q_{\alpha_{ext}}^i$ are external forces and torques, respectively. In addition to the obtained generalized mass matrix and force vector, it is necessary to determine the constraint equation through Lagrange multipliers λ. The procedure to obtain these constraint equations are well described in Shabana [8]. The constraint equation for the translation of the boom Λ_R and rotation of the boom Λ_θ are:

$$\Lambda_R^i = R^1 + A^1 d_{1i}^1 - R^i - A^i d_{i1}^i = 0$$
$$\Lambda_\theta^i = v^1 - A^i v^i = 0. \tag{10}$$

Vector d_{1i}^1 indicates the ith body attachment position written in BRF^i, v^i is a unit vector in $\Re^3$ pointing towards the boom rotation axis in BRF^i and $\Lambda^i = \begin{bmatrix} \Lambda_R^{i^T} & \Lambda_\theta^{i^T} \end{bmatrix}^T$. The generalized forces associates with the constraints, Q_c are determined by

$$Q_c = -\Lambda_{tt} - 2\Lambda_{qt}\dot{q} - (\Lambda_q \dot{q})_q \dot{q} \tag{11}$$

with the subscripts t and q indicating partial derivatives in respect to time and generalized coordinates, respectively. Equation 12 shows the final system of equation, where matrices without superscripts represents all the matrices concatenated. λ is in $\Re^{n_c}$ space, with n_c representing the total number of constraints in the system.

$$\begin{bmatrix} M & \frac{\partial \Lambda}{\partial q}^T \\ \frac{\partial \Lambda}{\partial q} & 0 \end{bmatrix} \begin{bmatrix} \ddot{q} \\ \lambda \end{bmatrix} = \begin{bmatrix} Q \\ Q_c \end{bmatrix}. \tag{12}$$

2.2 Structural model

In this work, the flexible booms are described using modal shaped obtained from the Euler-Bernoulli beam theory. The booms are considered cantilevered to the opening mechanism, so will be treated as such. As presented by Bigot and De Souza [11], the beam deflection motion can be obtained using the following equation

$$\frac{\partial^2}{\partial \zeta^2} \left(EI_2 \frac{\partial^2 \Omega(\zeta,t)}{\partial \zeta^2} \right) + \rho \frac{\partial^2 \Omega(\zeta,t)}{\partial t^2} = 0 \tag{13}$$

in which Ω is the vertical displacement of the beam and ζ a coordinate along its length. The Young Module, E, depends on the material, the second moment of area, I_2, depends on the geometry of the boom and ρ is the boom's density. For fixed free beams, the boundary conditions at the cantilevered end are $\Omega(0,t) = 0$ and $\frac{\partial \Omega(\zeta,t)}{\partial \zeta}|_{\zeta=0} = 0$. At the free end, the boundary conditions are $\frac{\partial^2 \Omega(\zeta,t)}{\partial \zeta^2}|_{\zeta=L} = 0$ and $\frac{\partial^3 \Omega(\zeta,t)}{\partial \zeta^3}|_{\zeta=L} = 0$.

Equation 13 can be solved by separation of variables, separating the spatial and temporal functions. This lead to the following shape functions Φ:

$$\Phi_k(\zeta) = A_k \left[\cosh\left(\frac{\alpha_k}{L}\zeta\right) - \cos\left(\frac{\alpha_k}{L}\zeta\right) - \sigma_k \left(\sinh\left(\frac{\alpha_k}{L}\zeta\right) - \sin\left(\frac{\alpha_k}{L}\zeta\right) \right) \right]. \tag{14}$$

Constants A_k and σ_k are determined for each mode shape as a function of α_k, which are the solutions of $\cos(\alpha)\cosh(\alpha) = -1$, and represents the kth mode. Lastly, σ_k is found through equation eq. (15).

$$\sigma_k = \frac{\sinh(\sigma_k) - \sin(\sigma_k)}{\cosh(\sigma_k) + \cos(\sigma_k)} \tag{15}$$

With the determined mode shapes, it is possible to generate the S matrix presented in the flexible multibody dynamics section, which is associated to the flexible body coordinates q_f.

2.3 Mechanisms model

As aforementioned, SPORT has four booms with spring mechanisms to open and maintain their final position. When deployed, the mechanism base structure limits the boom's maximum angular position, acting as a barrier. A virtual spring was considered in the model, in addition to the mechanism spring, to describe the boom collision with this structure. As explained by Wu and Chen [12], this method allows for the input of parameters to better describe the mechanism and collision behavior which can be determined experimentally. Hence, the torque τ is split in three terms

$$\tau = \tau_1 + \tau_2 + \tau_3 \tag{16}$$

where the first term, τ_1 is related with the mechanism spring

$$\tau_1 = \frac{P_1}{\Theta_r}\Theta_d \tag{17}$$

and $\Theta_d = \frac{\pi}{2} - \Theta$. The second term, τ_2 is related with the virtual spring, which is only active for $\Theta > \pi/2$:

$$\tau_2 = -\text{abs}(P_3(\Theta_r - \Theta))\text{u}(-\Theta_d). \tag{18}$$

Finally, the last term is related with the mechanism damping:

$$\tau_3 = -P_2\dot{\Theta}. \tag{19}$$

The constants P_j are parameters that will be further determined for each mechanisms, u is the unit step function, abs is a function to obtain the absolute value, Θ_r is the maximum angle each boom can reach (angle at which the boom collides with the mechanism barrier) and Θ is the boom's angular position relative to the HUB. Since there are considered only small deformations in the boom, and the collision occurs at its base, only the rigid body rotation angle is considered for determining when the impact occurs.

3 Simulation parameters and results

A simulation was conducted in order to evaluate the results obtained with generic coefficients for both mechanisms and structural parameters. All booms are considered to be solid circular beams of Al7076 T61 with Young Modules $E = 67$ GPa, Poisson $\nu = 0.33$, density $\rho = 2840$ kg/m^3 and an structural damping of 0.05 (these are not the real boom's parameters). The HUB mass is 8.5 kg and has the inertia matrix in eq. (20).

$$\bar{I}_{\theta\theta}^1 = \begin{bmatrix} 0.10477 & 0.003148 & 0.00098 \\ 0.003148 & 0.05858 & -0.001259 \\ 0.0009895 & -0.001259 & 0.134942 \end{bmatrix} \text{kgm}^2. \tag{20}$$

(a) E-Field +

(b) E-Field -

(c) SIP

(d) SLP
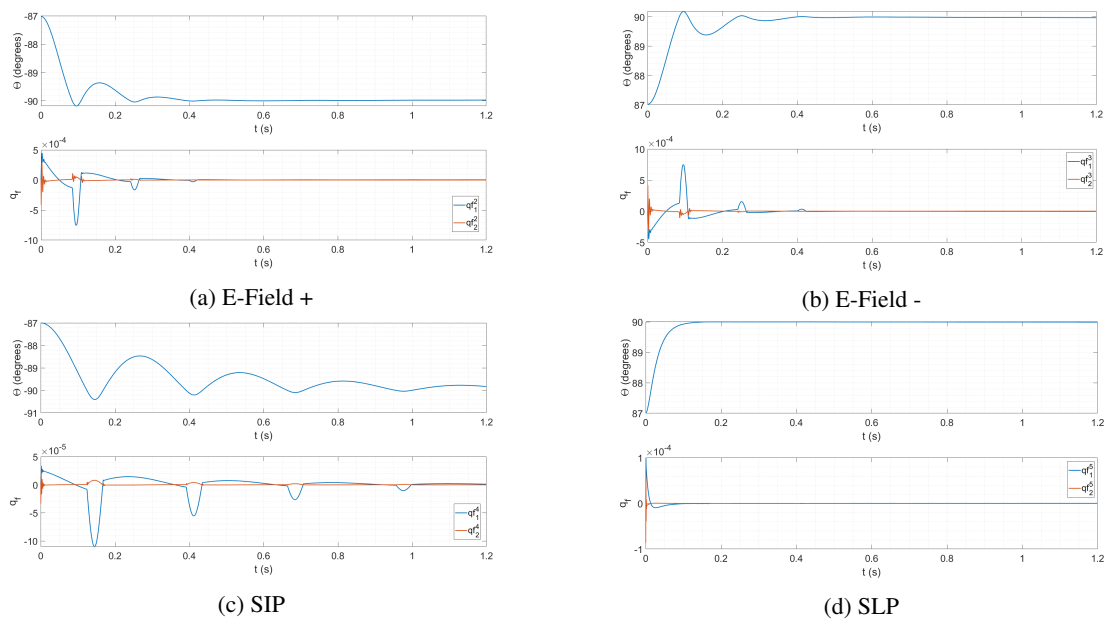
Figure 2. Boom's relative angular position and flexible body coordinates

Table 1 shows the mechanism parameters, boom's dimensions and its connection point with the HUB in the BRF^1 ($X^1Y^1Z^1O$).

Table 1. Simulation Parameters

Body	Length (m)	Diameter (m)	X^1 (m)	Y^1 (m)	Z^1 (m)	P_1 (Nm)	P_2 ($\frac{\text{Nms}}{\text{rad}}$)	P_3 ($\frac{\text{Nm}}{\text{rad}}$)	Θ_r (rad)
2	0.295	0.005	0.116	-0.151	0.029	0.35	0.01	10	$\pi/2$
3	0.295	0.005	-0.111	-0.151	0.029	0.35	0.01	10	$\pi/2$
4	0.302	0.01	0.091	-0.151	-0.053	0.25	0.01	10	$\pi/2$
5	0.146	0.005	0.069	-0.151	0.053	0.31	0.01	10	$\pi/2$

Applying a initial condition where all booms are $3°$ from their equilibrium position, it is possible to visualize the system dynamics in Figure 2, where $q_{f_1}^i$ and $q_{f_2}^i$ indicates the first and second modal shapes, respectively. The peaks in the flexible body coordinates corresponds to the boom's interaction with the virtual spring, as would be expected. The E-Fields had similar behaviors since they have the same parameters, with the elastic coordinates having opposite directions due to the orientation of the Z axis of each body (beam deflection occcurs in the ZY plane).

Figure 3 shows the HUB angular position - in the Local Vertical Local Horizontal Reference Frame, as explained by Wie [13] -, which displays the influence of the booms collision in the satellite attitude. This effect is more pronounced in the X^1 axis since two distinct mechanism rotate around it (SIP and SLP), in addition to the mechanism with biggest amplitude of oscillation (SIP). During maneuvers, this oscillatory behavior in the satellite attitude can impact the ADCS compromising its accuracy.

4 Conclusions

The proposed modeling was capable of simulating the interaction of the flexible boom, its mechanism, and the satellite HUB, which will allow the study of the SPORT boom's dynamics, ensuring a proper operation in orbit. Ongoing experimental research with the mechanisms will be used to estimate the coefficients of the spring model, providing a reliable model validated against experimental results. Further studies will be conducted in closed-loop simulations to analyze the impact of the calibration maneuvers on the satellite dynamics.
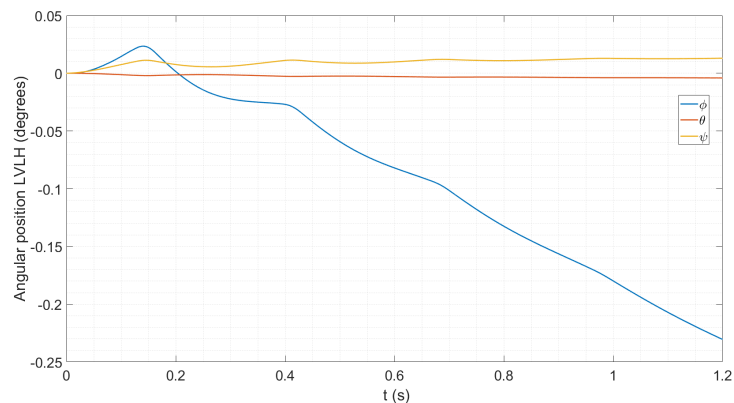
Figure 3. SPORT's HUB angular position in the Local Vertical Local Horizontal Reference Frame

Authorship statement. The authors hereby confirm that they are the sole liable persons responsible for the authorship of this work, and that all material that has been herein included as part of the present paper is either the property (and authorship) of the authors, or has the permission of the owners to be included here.

References

[1] Charles, S., Otávio, D., Luis, L., Heelis, & Rod, 2017. The Scintillation Prediction Observations Research Task (SPORT): An International Science Mission using a CubeSat. *31st Annual AIAA/USU Conference on Small Satellites*, pp. 8.

[2] Rong, B., Rui, X., Tao, L., & Wang, G., 2019. Theoretical modeling and numerical solution methods for flexible multibody system dynamics. *Nonlinear Dynamics*, vol. 98, n. 2, pp. 1519–1553.

[3] Luo, C. Q., Sun, J. L., Wen, H., & Jin, D. P., 2019. Dynamics of a tethered satellite formation for space exploration modeled via ANCF. *Acta Astronautica*.

[4] Ma, G., Xu, M., Liu, T., & Luo, Y., 2017. The multi-body analysis and vibration control of the second-order mode of a hoop flexible structure. *Acta Mechanica*, vol. 230, n. 4, pp. 1377–1386.

[5] Shi, C. & Wang, Y., 2016. Decoupled Tracking Control for a Flexible Multi-body Satellite with Solar Panels and Manipulator. In *Proceedings of 2016 Chinese Intelligent Systems Conference*, pp. 529–540. Springer Singapore.

[6] Liu, J. & Pan, K., 2016. Rigid-flexible-thermal coupling dynamic formulation for satellite and plate multibody system. *Aerospace Science and Technology*, vol. 52, pp. 102–114.

[7] Kong, W. & Tian, Q., 2020. Dynamics of fluid-filled space multibody systems considering the microgravity effects. *Mechanism and Machine Theory*, vol. 148, pp. 103809.

[8] Shabana, A. A., 2013. *Dynamics of multibody systems*. Cambridge university press.

[9] Schiavo, F., Lovera, M., & Astolfi, A., 2006. Magnetic attitude control of spacecraft with flexible appendages. *Proceedings of the IEEE Conference on Decision and Control*, pp. 1545–1550.

[10] Ferretti, G., Schiavo, F., & Viganò, L., 2005. Modular modelling of flexible thin beams in multibody systems. *Proceedings of the 44th IEEE Conference on Decision and Control, and the European Control Conference, CDC-ECC '05*, vol. 2005, pp. 3363–3368.

[11] Bigot, P. & De Souza, L. C., 2013. Design of non-linear controller for a flexible rotary beam using state-dependent riccati equation (SDRE) Control. *ICINCO 2013 - Proceedings of the 10th International Conference on Informatics in Control, Automation and Robotics*, vol. 2, n. 0, pp. 148–155.

[12] Wu, S.-C. & Chen, G.-S., 1993. Contact-Impact Analysis of Deployable Space Systems. In *34th Structures, Structural Dynamics and Materials Conference*, Reston, Virigina. American Institute of Aeronautics and Astronautics.

[13] Wie, B., 2008. *Space vehicle dynamics and control*. American Institute of Aeronautics and Astronautics.